

Document downloaded from the institutional repository of the University of Alcalá: <http://ebuah.uah.es/dspace/>

This is a posprint version of the following published document:

Alcover Sánchez, R., Soria Herrera, J.M., Pérez Aracil, J., Pereira González, E. & Díez Jiménez, E. 2022, "Design and experimental characterization of a novel passive magnetic levitating platform", Smart Structures and Systems, vol. 29, no. 3, pp 499-512.

Available at <https://dx.doi.org/10.12989/sss.2022.29.3.499>

© 2022 Techno Press

(Article begins on next page)



This work is licensed under a

Creative Commons Attribution-NonCommercial-NoDerivatives
4.0 International License.

Design and experimental characterization of a novel passive magnetic levitating platform

R. Alcover-Sanchez, J.M. Soria, J. Pérez-Aracil, E. Pereira and E. Diez-Jimenez*

Mechanical Engineering Area - Signal Theory and Communications Department,
Universidad de Alcalá, Ctra. Madrid-Barcelona Km 33.6 Alcalá de Henares 28805, Spain

(Received July 27, 2021, Revised November 9, 2021, Accepted November 18, 2021)

Abstract. This work proposes a novel contactless vibration damping and thermal isolation tripod platform based on Superconducting Magnetic Levitation (SML). This prototype is suitable for cryogenic environments, where classical passive, semi active and active vibration isolation techniques may present tribological problems due to the low temperatures and/or cannot guarantee an enough thermal isolation. The levitating platform consists of a Superconducting Magnetic Levitation (SML) with inherent passive static stabilization. In addition, the use of Operational Modal Analysis (OMA) technique is proposed to characterize the transmissibility function from the baseplate to the platform. The OMA is based on the Stochastic Subspace Identification (SSI) by using the Expectation Maximization (EM) algorithm. This paper contributes to the use of SSI-EM for SML applications by proposing a step-by-step experimental methodology to process the measured data, which are obtained with different unknown excitations: ambient excitation and impulse excitation. Thus, the performance of SSI-EM for SML applications can be improved, providing a good estimation of the natural frequency and damping ratio without any controlled excitation, which is the main obstacle to use an experimental modal analysis in cryogenic environments. The dynamic response of the 510 g levitating platform has been characterized by means of OMA in a cryogenic, 77 K, and high vacuum, 1E-5 mbar, environment. The measured vertical and radial stiffness are 9872.4 N/m and 21329 N/m, respectively, whilst the measured vertical and radial damping values are 0.5278 Nm/s and 0.8938 Nm/s. The first natural frequency in vertical direction has been identified to be 27.39 Hz, whilst a value of 40.26 Hz was identified for the radial direction. The determined damping values for both modes are 0.46% and 0.53%, respectively.

Keywords: cryogenics; dynamic response; levitating platform; magnetic damping; passive magnetic levitation

1. Introduction

Vibration isolation (VI) technique is used to reduce vibration transmitted from the supporting structure to the platform, where the payload is placed. For this purpose, an isolator is situated between the payload and the base. Thus, a controlled force is applied on the platform to reduce the vibration. The way in which the controlled force is generated determines the VI technique: passive vibration isolation (PVI), semi-active vibration isolation (SAVI) and active vibration isolation (AVI) (Preumont 2018).

There is a wide use of the VI techniques in different applications, such as precision equipment (Rivin 1995) or civil engineering (Casciati *et al.* 2012), where devices composed of on passive spring-damper, magnetorheological, or electro-inductive devices can be used. The use of PVI (Casciati and Giuliano 2009), SAVI (Casciati and Domaneschi 2007) or AVI (Bastais *et al.* 2009) depends on the required performance, the particular application and the environmental restrictions. Thus, it is common to find in the literature passive, semi-active and active applications.

The mentioned works may present tribological problems due to the low temperatures and/or cannot guarantee an enough thermal isolation. Magnetic levitation systems and magneto-mechanical components have been widely used in different structural applications where direct contact between structural elements shall be avoided (Siyambalapitiya *et al.* 2012). The lack of physical contact provides advantageous features like thermal isolation, vibration damping, frictionless and wall-through transmission of structural forces separation, which are very appreciated in many applications (Diez-Jimenez and Perez-Diaz 2011, Diez-Jimenez *et al.* 2017, Li *et al.* 2019, Perez-Diaz *et al.* 2014a or b).

Examples of use can be encountered in microelectronics manufacturing, in which the lack of contact allows frictionless systems and vibrationless and precision positioning of wafers (Busch-Vishniac 1990, Kumar *et al.* 2020). In biomedical applications, magnetic levitation technique enables the separation, measurement, and analysis of a wide range of materials and biosystems (Ashkarran and Mahmoudi 2020). Magnetic damping is also used in aerospace structures (Perez-Diaz *et al.* 2019). Other examples can be found in space satellites cryostats for separating cold parts with high sensitivity sensors from warm parts (Riabzev *et al.* 2009).

Magnetic levitation systems can be also distinguished

*Corresponding author, Ph.D., Professor,
E-mail: cfren.diez@uah.es

between passive, semi-active and active. Active systems can provide larger stiffness and damping capacities, whilst the dynamic properties of the system can be changed during the simulation (Choi and Gweon 2011, Olaru *et al.* 2017). Passive magnetic levitation does not require control electronics, thus no power source is required. However, passive magnetic levitation systems may require an optimization process for practical uses since the stiffness capacity is limited. Passive magnetic levitation systems are usually composed of diamagnetic materials, like graphite or superconducting materials. Semi-active technique can bring the best of passive devices (their reliability) and the best of active devices (their versatility and adaptability). They are convenient in many levitation applications, as shown in (Ohashi and Ueshima 2012). SML dynamic parameters can be tuned in different ways. For example, the cooling position determines final dynamic parameters. Another option is to inject current in the superconducting materials themselves. In addition, placing coils around the magnets would also allow changing the controlled force of the VI, emulating an active VI technique (Ma *et al.* 2003).

Active, semi-active and passive techniques can provide structural vibration damping (Ghodsi *et al.* 2019, Jamshidi *et al.* 2017) and even energy harvesting (Park and Jang 2020, Shen *et al.* 2016). Also, they can provide negative stiffness, which is a very desired feature in smart structures for vibration damping (Diez-Jimenez *et al.* 2019a or 2021).

The use of passive levitation systems and Superconducting Magnetic Levitation (SML) has generated a great interest. (Diez-Jimenez *et al.* 2018, Perez-Diaz *et al.* 2015, Valiente-Blanco *et al.* 2014). SML consists of one cold part (superconductor piece) and one warm part (permanent magnet element). Meissner interaction and flux trapped of type II superconductors provide a stable levitation position of the permanent magnet without the need of any control (Perez-Diaz *et al.* 2012, Valiente-Blanco *et al.* 2013). An additional advantage of SML is that the system can be thermally rebooted as many times as needed. If there is an issue with the alignment of the platform, the system can be heated up and cooled down again, and the platform will be again in the right initial position (Perez-Diaz *et al.* 2014a or b, Valiente-Blanco *et al.* 2015). However, the cryogenic temperature required in the cold part prevents its extensive application in other fields.

SML has been widely applied in rotational and linear bearings system to avoid tribological issue that appears as such low temperatures (Cansiz 2009, Hull 2000). However, the use of SML as structural and vibration damping support has been scantily explored. A demonstration of magnet-superconductor for vibration damping was analyzed in (Yu *et al.* 1999). In that work, damping coefficients were measured for a single not-optimized magnet-superconductor pair. A SML prototype, where a cryogenic Liquid Nitrogen (LN2) tank is used as supporting structure, is presented in (Gauss *et al.* 1999).

The first contribution of this paper is the proposal of a contactless vibration damping and thermal isolation platform based on a three-legged SML structure, which

guarantees VI and levitation over the six degrees of freedom. The three SML supports act as three supporting legs of a flat levitating platform. The presented design exhibits high stiffness and damping coefficient levitation, being able to operate in cryogenic environments. This prototype can be classified as PVI system, which must be dynamically identified to characterize its frequency response.

The second contribution of this work is related to dynamic identification of the frequency response using Operational Modal Analysis (OMA) technique. Due to the fact that OMA does not need any controlled excitation force, it has been widely used for structure identification (Chang and Chou 2020, Lee *et al.* 2019), such as bridges and large buildings (Jiménez-Alonso *et al.* 2019, Kaloop *et al.* 2020, Niu *et al.* 2012). The use of OMA is very convenient to dynamically characterize SML systems since only just few sensors are required. In addition, it has low interaction with the levitating system, also showing high reliability. Although, these features are very appreciated for those tests developed inside a vacuum chamber and in extreme temperatures, where any restart in the thermal-vacuum process implies days of laboratory preparation, OMA technique was not originally developed for magnetic levitation characterization.

The methods available to perform the identification of modal parameters of dynamic systems based on OMA are usually classified as frequency or time domain methods, which have been extensively studied in the literature (Andersen 1997, Jacobsen *et al.* 2008, MacLamore *et al.* 1971, Van Overschee and De Moor 1996, Zhang *et al.* 2009). However, the current OMA-related techniques are still evolving, with the aim of achieving better estimations. One of these techniques is the OMA based on Stochastic Subspace Identification (SSI) methods using the Expectation Maximization (EM) (Cara *et al.* 2012). SSI-EM introduces the EM algorithm (McLachlan and Krishnan 2007) to maximize the likelihood function, which optimizes the lack of optimal solution shown by Bauer (2005) and Chiuso and Picci (2004) and improves the SSI results, discarding the spurious modes that appear in high order models and discovering other hidden modes.

The contribution of this work is the proposal of a step-by-step experimental methodology based on the SSI-EM, which was firstly shown in Cara *et al.* (2012). This methodology processes the measured data, improving the accuracy of Cara *et al.* (2012) for this application. Thus, two different unknown excitations: ambient excitation and impulse excitation, are used to obtain a good estimation of the natural frequency and damping ratio of the system. Controlled excitations have not been used, hence avoiding the main obstacle in the experimental modal analysis in cryogenic environments. The experimental characterization shows that the passive levitation system has acceptable load capacity and stiffness, and good vibration damping properties. Therefore, the proposed SML prototype can be used in cryogenic applications where contactless, thermal isolation and vibration damping are required.

This work continues with the design of the levitating platform. Section 3 describes the mathematical model of the

passive isolator, which is used in the OMA to identify the mechanical stiffness and damping. Section 4 explains how the system has been manufactured and assembled. Section 5 presents the test setup and Section 6 and 7 show the results and main conclusions of this work, respectively.

2. Design and analysis of the levitating platform

This section describes the first contribution of this work: the contactless vibration damping and thermal isolation platform based on a three-legged SML system. This design is divided into two main paths: mechanical design and electromagnetic design. The mechanical design is oriented to assure a good platform stability while being compact. The design is based on a three supporting legs topology, providing a plane of stability, and guaranteeing VI over six degrees of freedom. The electromagnetic design has been done with the aim of optimizing the stiffness of each supporting point while reducing the total amount of magnetic parts.

2.1 Mechanical and electromagnetic design

The design of the levitating platform includes the following three main elements (see Fig. 1): (i) levitating platform, (ii) 3 magnet-superconductor bearing pairs and (iii) LN2 cold plate tank. Note that the coordinate system, which is used to better illustrate the different views of the prototype, is depicted in Fig. 1 (isometric view). The Z direction is normal to the XY plane.

The levitating platform is a cylindrical plate with a set of M6 threaded holes to attach the sensors and other parts. These threaded holes are placed in a 20×20 mm grid along the plate. The external diameter is 180 mm and thickness 6 mm. This part is manufactured in aluminum 6061.

The levitation of the platform is achieved by using three magnet-superconductor bearing pairs. The three bearing pairs are symmetrically attached to the levitating platform

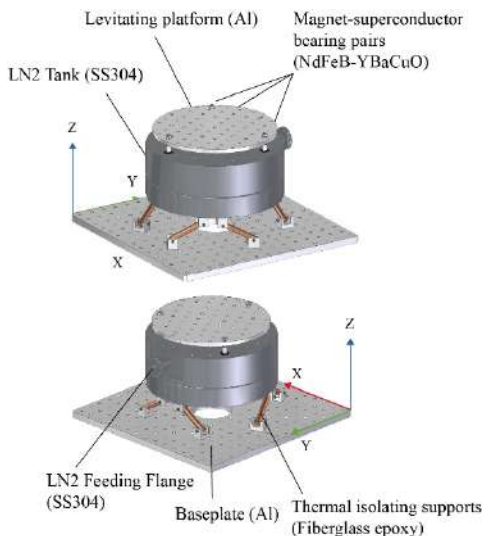


Fig. 1 Isometric views of the 3D mechanical model

in 120° distribution and in a radius of 80 mm from the center. Each of these pairs of bearings consist of two cylindrical permanent magnets and three cylindrical high temperature superconductors, as shown in Fig. 2.

The permanent magnets are hollowed cylinders with 7 mm outer diameter, 1.5 mm inner diameter and 9 mm height. They are made in NdFeB N50 with standard Ni coating. Permanent magnets are axially magnetized, and they are assembled with opposite magnetization directions. In this way, the stiffness is maximized as demonstrated in Valiente-Blanco *et al.* (2014). However, the assembly becomes more difficult as magnets tends to repel each other. Thus, adhesive must be used to keep the magnets north faces one against the other. We have used STYCAST 2850KT epoxy resin as adhesive because the good performance at low temperature. In addition, a titanium grade 5 1.5 mm diameter rod has been inserted in the inner magnet diameter to keep the magnets aligned while the epoxy is curing. This titanium rod also serves as link with and M4 screw that fasten the magnet stack to the aluminum levitating plate, depicted in Fig. 2. Aluminum plate plus the three magnet stacks elements composes the part that is levitating.

The levitating plate including the magnet stack is going to be the suspended mass of the levitating system. Therefore, it is important to analyze the vibrational modal behavior of this levitating part separately from the magnet-superconductor bearing pair to discard any possible interaction between modal response of the levitating solid and modal response of the contactless magnetic support.

The modal response of this plate has been simulated using Finite Element Model (FEM), with ANSYS Mechanical software v2020. A simplified geometrical model of the plate and magnets stack has been done. The simulation results show a first natural frequency of 827.66 Hz and a second of 828.26 Hz. These values are well far from the resonance frequencies of the whole system. Deformation results and frequencies for the first two natural frequencies are shown in Fig. 3.

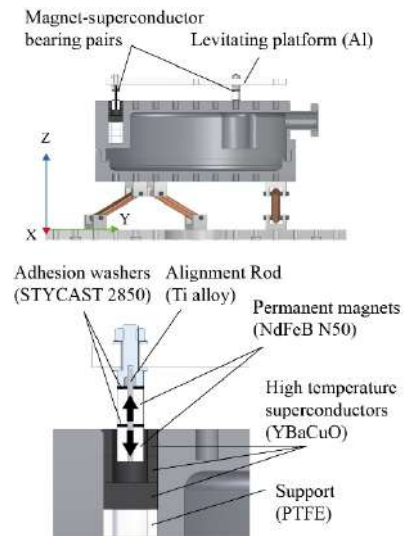


Fig. 2 Cross section of the LN2 tank (top) and detailed view of the magnet-superconductor bearing pair (bottom)

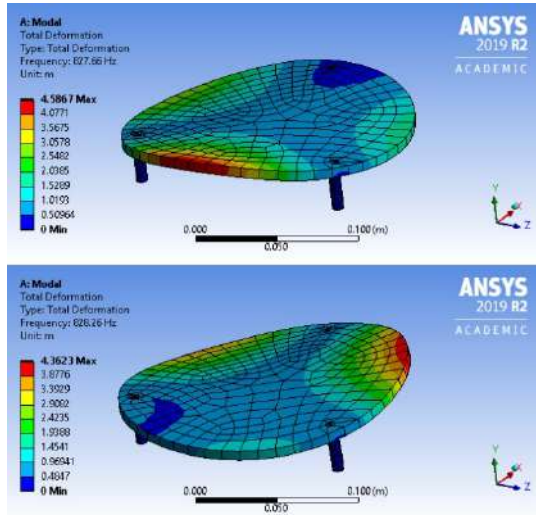



Fig. 3 First (827.66 Hz) and second (828.26 Hz) vibration eigenmodes from FEM simulation

High temperature cylindrical superconductors made in YBaCuO are used in the bearing pair static part. This material becomes superconductor at temperatures lower than 92 K. Three superconducting cylinders are stack together to create a housing that surrounds the magnet. Two of these cylinders are hollowed cylinders with 14 mm outer diameter, 9 mm inner diameter and 7 mm height. The bottom superconductor is a full cylinder with 14 mm diameter and 7 mm height. Therefore, the radial air gap between magnet and superconductor is set in 1 mm. All dimensions of the magnet-superconductor bearing pair are shown in Fig. 4.

As superconductors must operate in cryogenic temperature, it is needed to include a cool down system. The design includes a LN2 tank, which is a cold plate designed to achieve the following requirements: low thermal conduction between tank and baseplate, easy manufacturing and assembly, stability of orientation and position, high first natural frequency and non-magnetic response. All details of the LN2 tank design, and its structural modal characterization are given in reference (Díez-Jiménez *et al.* 2019a or b).  described in that

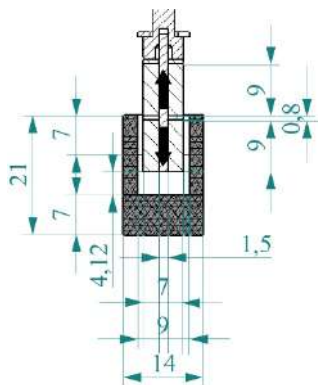


Fig. 4 Dimensions of the magnet-superconductor bearing pair and magnets magnetization directions (in black arrows)

reference, the first natural frequency of the LN2 tank appears at 115 Hz. This frequency is far from the natural frequencies of the levitating platform support.

Superconductors are inserted into dedicated holes in the LN2 tank, as shown in Fig. 2, cross section. Polytetrafluoroethylene (PTFE) supports are also inserted in the holes to elevate the position of the superconductors. In this way, if the liquid nitrogen the liquid nitrogen (77 K) is poured into the tank, superconductors are cooled down below their transition temperature (92 K).

High temperature cylindrical superconductors made in YBaCuO are used in the bearing pair static part. This material becomes superconductor at temperatures lower than 92 K. Three superconducting cylinders are stack together to create a housing that surrounds the magnet. Two of these cylinders are hollowed cylinders with 14 mm outer diameter, 9 mm inner diameter and 7 mm height. The bottom superconductor is a full cylinder with 14 mm diameter and 7 mm height. Therefore, the radial air gap between magnet and superconductor is set in 1 mm. All dimensions of the magnet-superconductor bearing pair are shown in Fig. 4.

Besides the levitation platform parts, SML always requires an auxiliary lock and release system. This system must hold the levitating elements in relative position against the superconductors while cooling down. The lock and release mechanism designed in composed of three locating pins placed close to the magnet-superconductor pairs as shown in Fig. 5. These locating pins provides separation between the levitating platform and the LN2 tank. The locating pins can be removed automatically by means of a rotary servo actuator. Servo actuators selected are three Towerpro MG995 model commercially available with small adaptation for its operation in vacuum environment. This small adaptation consisted juts in some small, drilled hole in the bottom part that permits the vacuum pump to quickly remove the inner air. Servo actuators are connected to the base plate through aluminum profiles.

2.2 Analysis and electromagnetic simulation of the superconductor magnetic levitation

The analysis and simulation of superconductor materials is complex. The magnet-superconductors forces in the

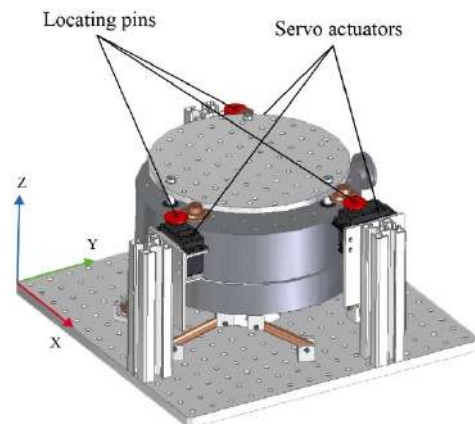


Fig. 5 Lock and release mechanism design

mixed state can be estimated by some analytical and FEM approximations, which considers the current density limits. However, these models are extremely sensitive to material crystal orientations and their electromagnetic properties. In the particular cases of polycrystalline YBaCuO superconductors, the estimation of forces a priori is usually carried out by model adjustment after test measurements.

This section proposes an analysis to obtain the estimation of these forces by considering of: (i) the repulsion force caused by the Meissner effect and (ii) the attraction force caused by trap field. When a superconductor is operating in the mixed state, as in current application, there are two phenomena superposing their magnetic response: Meissner effect magnetic field repulsion and trap field where some field lines are captured in the superconductor material volume. By combining the calculations of forces in those two states, the total levitation force and stiffness behavior can be obtained.

On the one hand, Meissner effect is the total expulsion of any magnetic field from the superconductor volume. This is a repulsion force of any magnet against any superconductor, therefore, a negative stiffness. This effect can be simulated by considering the superconductor material as a pure diamagnetic material with a magnetic permeability near to zero, i.e., $\mu_r = 0.001$ or smaller.

On the other hand, trap field of the mixed state of the superconductor can be simulated by considering the superconducting volume as having a high magnetic permeability, as for example, the one of the iron. This generates attraction of the magnets against the superconductor simulated materials. A positive stiffness can be also determined.

This combined simulation technique has been applied for one magnet-superconductor bearing pair of the levitating platform. It has been simulated in a 2D axisymmetric model. All simulations have been done using ANSYS Electronics 2020 R1, software. The solver chosen

is the magneto-static solver. The magneto-static field solution verifies the Maxwell's equations. As boundary conditions a "Zero tangential Field" type condition is applied in the external edges of the surrounding region volume. No current or field excitation is used, only permanent magnetization and two different magnetic permeabilities for the superconductor.

Forces and torques are calculated by applying the virtual forces principle. The mesh is refined to achieve less than 1% of energy error within a simulation time shorter than 20 seconds per run. All the simulations have been run on a computer with an Intel Core i4-4690, RAM memory 8Gb.

Fig. 6 shows the magnetic field distribution of magnets-superconductor bearing pair in a pure Meissner state. Simulation have been done in the exact cooling position-height. No magnetic field penetrates inside the superconducting volume. The calculation of the vertical force on the magnets returns a value of +5.2 N, which means a vertical repulsion force that will compensate the weight force.

Fig. 7 represents the magnetic field distribution of magnets-superconductor bearing pair with some magnetic field penetrating. Simulation have been done in the exact cooling position-height and considering the trapping field effect as if it was iron. The magnetic field penetrates inside the superconducting volume and therefore, there is an attraction. The calculation of the vertical force on the magnets returns a value of -2.8 N, which means a vertical attraction of the magnets against the superconducting volume.

By combining both solutions, we can determine that there will be a vertical force capacity of 2.4 N upwards at each bearing pair. The total weight of the suspended mass, which is $W = 0.51 \cdot 9.8 = 4.99$ N. This weight will be distributed between the three bearing pairs, so each bearing pair must hold 1.66 N. Therefore, the electromagnetic design seems to be in similar order of magnitude of the

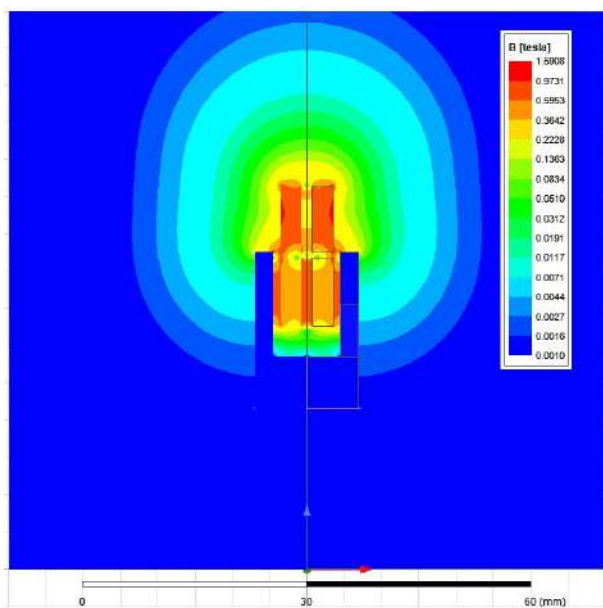


Fig. 6 Magnetic field distribution of magnets-superconductor bearing pair in a pure Meissner state

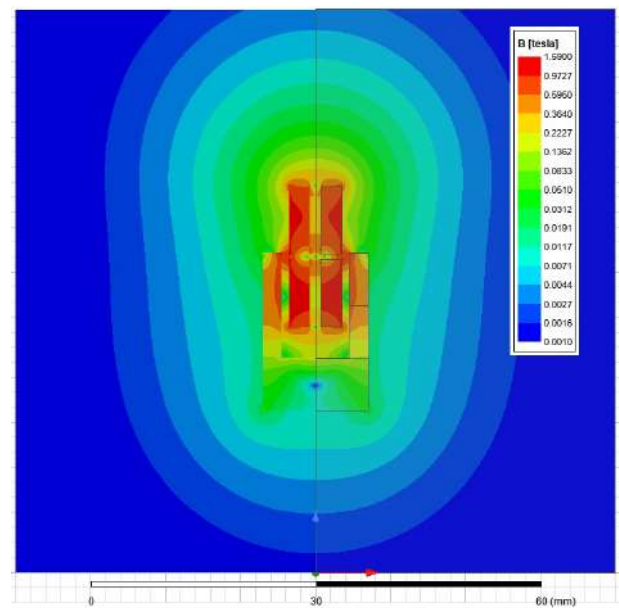


Fig. 7 Magnetic field distribution of magnets-superconductor bearing pair in a mixed state

necessary capacity, although the model shall be corrected after test. The next step is to characterize the dynamic behavior of this SML, whose static force guarantee the levitation of the platform.

3. Dynamical model

This section describes the simplified dynamical model of the SML passive levitation system. The FEM analysis carried out in Section 2 shows that the lowest frequencies of the plate are around 800 Hz. The resonant frequencies (vertical and radial) are expected to be below 50 Hz. Thus, the model can be considered as a rigid plated placed on three SML legs (see Fig. 8) because the interaction of system is negligible. In addition, the hypothesis of small displacements is considered for both directions, vertical and radial. Thus, the levitation system can be considered as a passive isolator of 2 degrees of freedom with two main vibration modes. Viscous damping is considered for the system since this model can provide an accurate response of the passive isolator. Thus, it is not needed to consider hysteretic damping (Zeynalian *et al.* 2012).

The magnetic levitating platform can be modeled as a rigid plate located on three supporting legs. The platform is instrumented with two accelerometers situated at the center of the cold plate. These accelerometers can measure the vertical and radial acceleration, which are denoted as \ddot{x}_v and \ddot{x}_r , (see Fig. 8). It is considered that the three SML legs are the same.

Each leg is modelled as a two degree of freedom system (see Fig. 9). The dynamic parameters of each leg are shown in figure E2. Note that each high stiffness SML rotational bearing is considered as a linear system with vertical and radial stiffness (k_r and k_v) and viscous damping (c_r and c_v), which levitates a mass m_p . The total vertical and radial parameters is found by multiplying by three. The total mass of the cold plate and the objects placed on it is $3m_p$.

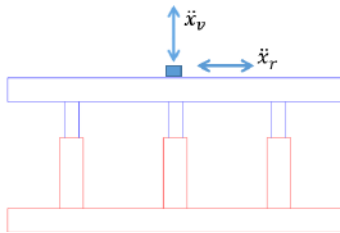


Fig. 8 Schematic frontal view of the magnetic levitation platform

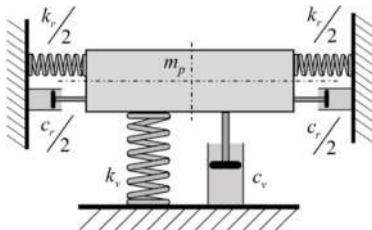


Fig. 9 Dynamic isolation system model

Under the hypothesis of small displacements for both directions vertical and radial, the damping coefficient and the natural frequency of each leg are equal to those of the levitation platform. Thus, if the system is considered to be linear and homogenous, the differential equation of each leg, which models the force exerted on the base, can be analogous to the differential equation that considers the forces imparted by the isolation platform on the base. Thus, the governing equations of motion in vertical and radial directions are expressed as follows

$$-c_v(\dot{x}_v(t) - \dot{x}_{bv}(t)) - k_v(x_v(t) - x_{bv}(t)) = m_p \ddot{x}_v(t) \quad (1)$$

$$-c_r(\dot{x}_r(t) - \dot{x}_{br}(t)) - k_r(x_r(t) - x_{br}(t)) = m_p \ddot{x}_r(t) \quad (2)$$

The variables x_{bv} and x_{br} denote the vertical and radial displacements of the ground (i.e., hot plate), respectively. Then, the transfer functions (TFs) from the base structure motion to the platform motion, in vertical and radial directions, can be expressed as follows

$$G_{iv}(s) = \frac{s^2 X_v(s)}{s^2 X_{bv}(s)} = \frac{2\xi_v \omega_v s + \omega_v^2}{s^2 + 2\xi_v \omega_v s + \omega_v^2} \quad (3)$$

$$G_{ir}(s) = \frac{s^2 X_r(s)}{s^2 X_{br}(s)} = \frac{2\xi_r \omega_r s + \omega_r^2}{s^2 + 2\xi_r \omega_r s + \omega_r^2} \quad (4)$$

where s is the Laplace variable and capital letters indicate the Laplace transforms of the variables. The parameters ξ_v and ω_v are the damping ratio and natural frequency in the vertical direction, respectively, which can be obtained from these relationships $\frac{c_v}{m_p} = 2\xi_v \omega_v$ and $\frac{k_v}{m_p} = \omega_v^2$. Analogous to vertical direction, the damping ratio (ξ_r) and the natural frequency (ω_r) in the radial direction can be obtained from $\frac{c_r}{m_p} = 2\xi_r \omega_r$ and $\frac{k_r}{m_p} = \omega_r^2$. Thus, if the natural frequencies (ω_v and ω_r) and the damping coefficients (ξ_v and ξ_r) are obtained by the OMA, and the value of m_p is known, the stiffness and viscous damping can be obtained as follows

$$k_v = m_p \omega_v^2 \quad \text{and} \quad k_r = m_p \omega_r^2 \quad (5)$$

$$c_v = 2m_p \xi_v \omega_v \quad \text{and} \quad c_r = 2\xi_r \omega_r m_p \quad (6)$$

Note that the OMA can obtain the poles of $G_{iv}(s)$ and $G_{ir}(s)$ by analyzing the signals $\ddot{x}_v(t)$ and $\ddot{x}_r(t)$ under any unknown excitation.

4. Manufacturing and assembly

The manufacturing and assembling of the experimental system have been carried out at the Manufacturing Workshop Universidad de Alcalá. Some of the pieces have been fabricated using Computer Numerical Control (CNC) machine, while some of the standard and magnetic pieces have been purchased to external suppliers. The nitrogen

deposit, Fig. 10, was manufactured in two pieces welded at the manufacturing laboratory. In addition, there were included the legs for the thermal isolation, screwed by the hinges. Further details are shown in [34].

The levitating platform with the three legs already assembled in the structure is shown in Fig. 11. The location of the permanent magnets was chosen to be placed at 120 degrees orientation respect to the axes of symmetry.

These permanent magnet legs have been manufactured from a M4 screw with through hole where a 1.5 mm



Fig. 10 LN2 Tank Manufactured and ready for assembling

diameter titanium bar was inserted and fixed with the STYCAST 2850KT epoxy resin. After the bar was well fastened to the screw, the magnet attachment started. It is done by inserting the first magnet, with an arbitrary polarity, and then the second magnet with the opposite polarity. Since the different polarities made the two magnets repelling each other, there were built some plastics molds to hold them meanwhile the resin cures properly. After the curing time was reached, the bases were unattached and the whole piece became a rigid solid, as shown in Fig. 12. The three legs were now linked to the levitant platform.

Superconducting rings and cylinders were purchased to CAN superconductors, directly with the required dimensions, Fig. 13. Before inserting them, superconductors were covered with vacuum grease Apiezon to protect them against any oxidation or reduction that could happen on their surfaces. Once coated, they were inserted in their holes. The superconductors were inserted in the deposit and the whole deposit was in the vacuum chamber as shown in Fig. 14.

The vacuum chamber must always be cleaned with alcohol on all its surfaces to minimize the outgassing of all the elements located inside. In addition, all the cables were

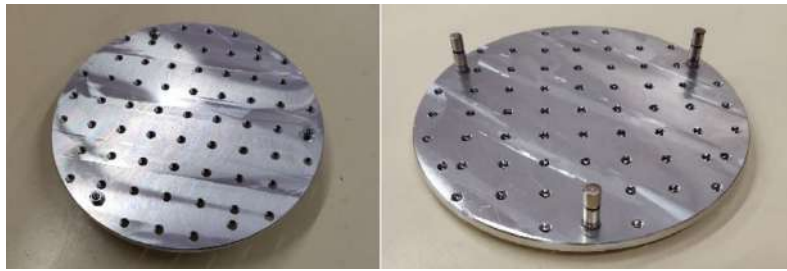


Fig. 11 Levitant platform with the three permanent magnets stuck assembled (left) and bottom view (right)



Fig. 12 Detail of the permanent magnets glued

connected through the electrical feedthroughs and placed along the vacuum chamber. The three elements of the lock and release mechanism were installed to enable the support of the levitant cap during the cooling until reaching cryogenic temperatures. At this point of the assembling, the three columns with their correspondent's servo motor were located and screwed to their supports.

Finally, and as shown in Fig. 15, the levitant platform was located and the position of the servo motors were adjusted. By this way, when activating the servo motors, the stops will release the levitant platform free to levitate by itself. The levitant platform was aligned with respect to the



Fig. 13 Superconducting rings and superconducting cylinder from CAN superconductors



Fig. 14 LN₂ Tank with the superconductors located inside the Vacuum chamber



Fig. 15 Detailed view of the final position of the permanent magnet in respect of the superconductor

superconductors, assuring that the airgap between the permanent magnets and the superconductors had a value of 1 mm, Fig. 15. For a more precise fit, some cylindric gauges were inserted between the permanent magnets and the superconductors meanwhile the stops were being installed. After the stops were located, the gauges were removed for initiating the vacuum and cooling process.

5. Test setup and procedure

Dynamic response of the levitating platform must be tested inside a cryogenic and vacuum environment. This type of devices can hardly operate in ambient pressure because the cryogenic parts tend to condensate water in their surroundings and so it can block the levitation. Therefore, the device has been mounted inside a high vacuum chamber together with a set of vacuum and cryogenic compatible sensors as describes next.

The chamber has six DN35CF flanges and one bottom flange for the vacuum pump, as shown in Fig. 14. Two of the flanges were used as electrical feedthrough connectors, using two D-Sub 50 ports. A third flange was used to connect a pressure sensor. A fourth flange was used to connect a manual vent valve. The fifth flange was used as a feedthrough port for 4 BNC coaxial cables. The last available flange was used as a pipeline to feed the external LN₂ supply. The bottom flange was connected to a turbo-pump station with a turbo-molecular nEXT85H pump attached to an XDD1 dry diaphragm backing pump from Edwards Company.

LN₂ was manually fed via a plastic thermal isolated pipe inserted into the corresponding flange. This plastic

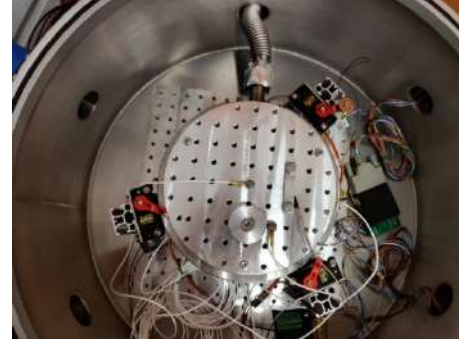


Fig. 16 Temperature sensor and vibration sensors installed on the levitating platform surface

pipe was surrounded by a flexible hermetic bellow screwed to the DN16CF LN₂ vessel flange. All the CF flange connections were done using a copper gasket, coated with vacuum-compatible grease.

One temperature sensor and two accelerometers have been attached to the top surface of the levitating platform to measure temperature and vibration conditions. Accelerometers are mounted to measure in vertical and horizontal directions, as shown Fig. 16.

The sensing system includes temperature, pressure, and acceleration measurements. The temperature was measured using several PT100 platinum resistance probes wired in a four-wire bridge configuration. Temperature measurements were acquired using USB-6211 data acquisition system from National Instruments and using a personal computer with LabVIEW software. Three PT100 sensors were used: PT100-1, place at the base of the whole device; PT100-2, attached to the top surface of the LN₂ tank and PT100-3 placed in the levitating platform. All PT100 sensors were encapsulated using Apiezon thermal-vacuum grease to assure a correct thermal contact. KJLC (Jefferson Hills, PA, USA) cold cathode/Pirani gauge pressure was used to measure the pressure inside the vacuum chamber. Data logging of the pressures were done manually.

The CompactDAQ-9191 data acquisition unit and NI-9234 input module by National Instruments were used to acquire the data. The monitoring system comprises 3 IEPE accelerometer channels. The frequency sampling for each channel was chosen to be 1651.61 Hz, enough to identify the modal parameters of the system and to avoid aliasing problems during postprocessing.

The accelerometers used for OMA were two IEPE 3035B uniaxial accelerometers (DYTRAN, Chatsworth, CA, USA) with a sensitivity of 100 mV/g, a frequency response of 0.5–10000 Hz, and a mass of 2.5 g. Both accelerometers were placed at the levitating platform in vertical and horizontal orientation correspondingly.

6. Results

Tests started after reaching the vacuum and cryogenic temperature by connecting vacuum pump and by feeding with LN₂ the superconductors container. Once the vacuum level inside the chamber reached around 1E-3 mbar, LN₂

pouring started. By cooling down the LN2 tank, the inner pressure still dropped down to 1E-5 mbar, operative point. When temperature sensors indicated that superconductor were at around 77 K, then, lock and release mechanism released the platform to levitate freely, and dynamic characterization started.

First, the natural frequencies and damping ratios are analyzed by classical OMA technique. This paper proposes a step-by-step experimental methodology to process the measured data. The first step is to analyze, in the frequency domain, the acceleration measured for ambient excitation. Figs. 18 and 19 shows a time-frequency spectrogram map of the raw vertical and horizontal accelerations, respectively, of the platform for the ambient vibration test. The duration of the acceleration data is 300 seconds and the sampling frequency is equal to 1651.61 Hz.

A second approximation uses a 100 seconds signal. This signal is measured with external non-measured impulse excitation and sampling frequency equal to 1651.61 Hz. In addition, the signals are filtered by a low-pass fourth-order

Butterworth filter with a cut-off frequency of 48 Hz. In this approximation, one of the signal peaks from the unmonitored hits data is picked. Thus, the value of the vibration frequency is obtained measuring the distance between peaks from one of the hits. In addition, the damping ratio is estimated by means of the logarithmic decrement method. This procedure for estimating frequency and damping is an appropriate method when the response is caused by only one vibration mode and there is no other closed-frequency vibration mode. The signal processing allows the correction of slight deviations. Thus, the decays measured after the application of the force should contain only the contribution of a single mode.

Fig. 19 shows both raw and processed acceleration responses in vertical direction (a) and a zoom view of the response from one of the hits (b). The frequency and damping ratio values are obtained from the selected points represented in Fig. 19, thus resulting 27.36 Hz and 1.19%, respectively. In the same way, Fig. 20 shows the radial acceleration. The values obtained for the frequency and

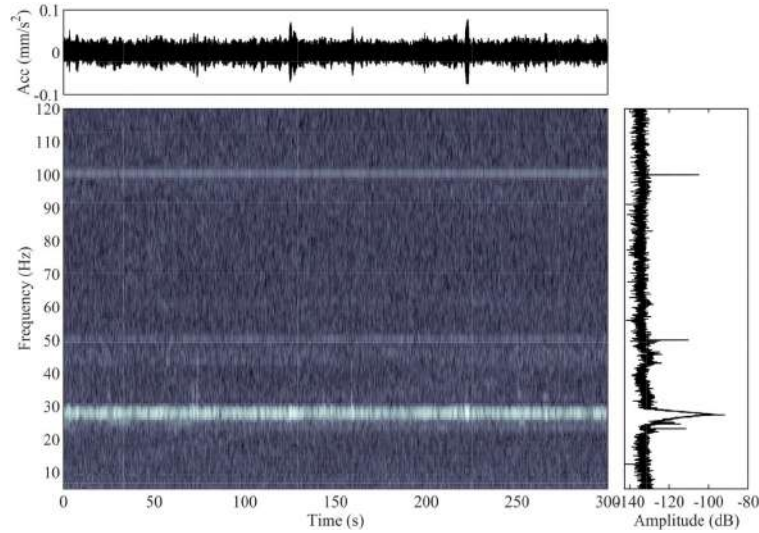


Fig. 17 Time-frequency spectrogram of vertical response

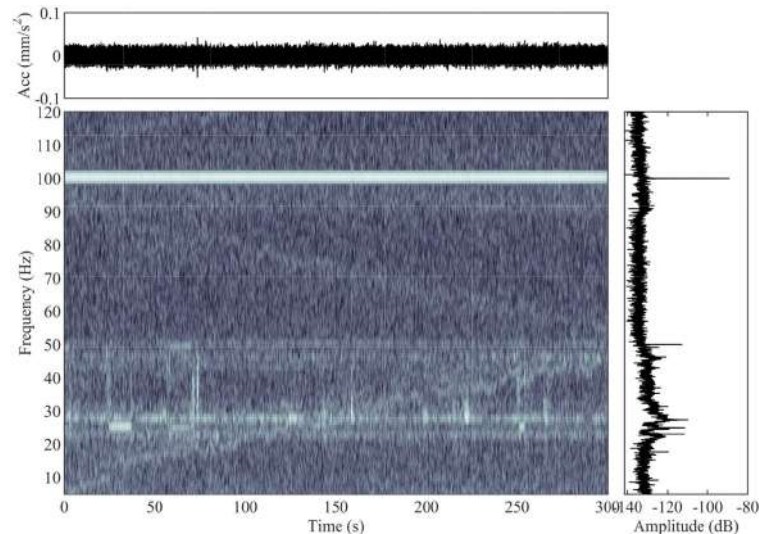


Fig. 18 Time-frequency spectrogram of horizontal response

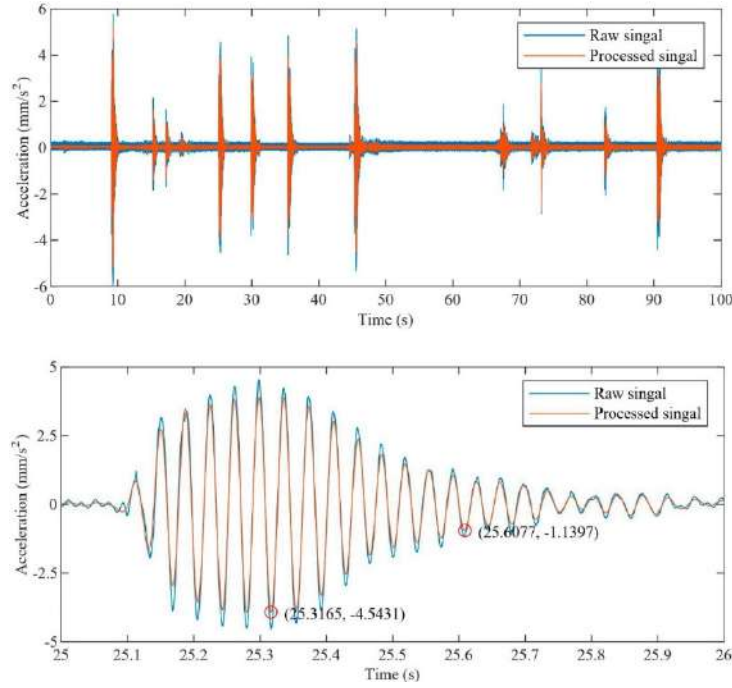


Fig. 19 Free decay vertical response after non-measured impulse. (o) Selected points to compute zero crossing frequency and logarithmic decrement

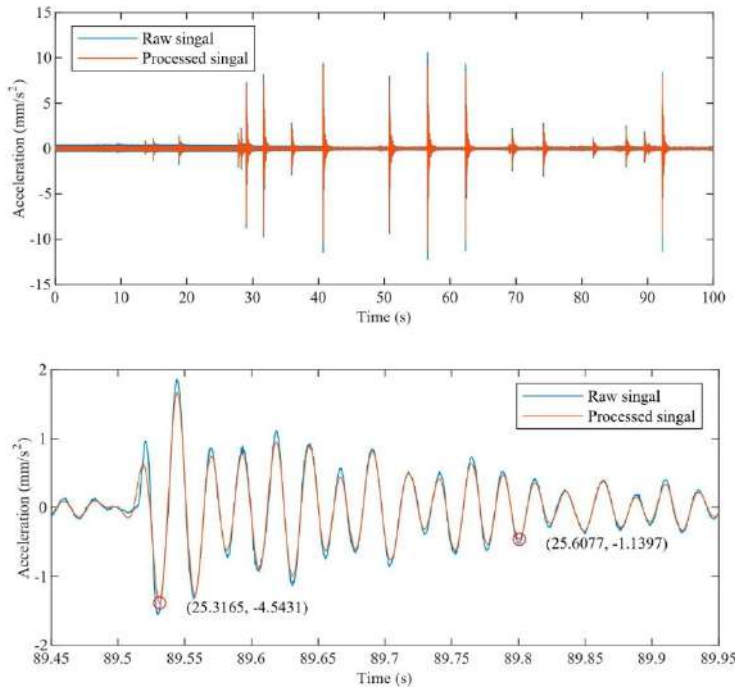


Fig. 20 Free decay horizontal response after non-measured impulse. (o) Selected points to compute zero crossing frequency and logarithmic decrement

damping ratio, in the radial direction, have been 40.98 Hz and 1.83%, respectively. It is important to note that, although the radial direction has experienced a noisier response, it has been possible to obtain the natural frequency and damping coefficient values. However, these modal parameters estimation are less accurate than the parameters of vertical direction.

The last approach uses both ambient and impulsive

excitations. Both signals are now filtered by a high-pass fourth-order Butterworth filter with a cut-off frequency of 0.1 Hz. Thus, the mean and drift are eliminated. Also, the signal is filtered by a low-pass fourth-order Butterworth filter of with a cut-off frequency of 48 Hz. A decimation factor of 14 is applied, and a Nyquist frequency of 58.98 Hz is obtained. These signals are used with the SSI-EM.

This SSI-EM based on the SSI and EM algorithms is

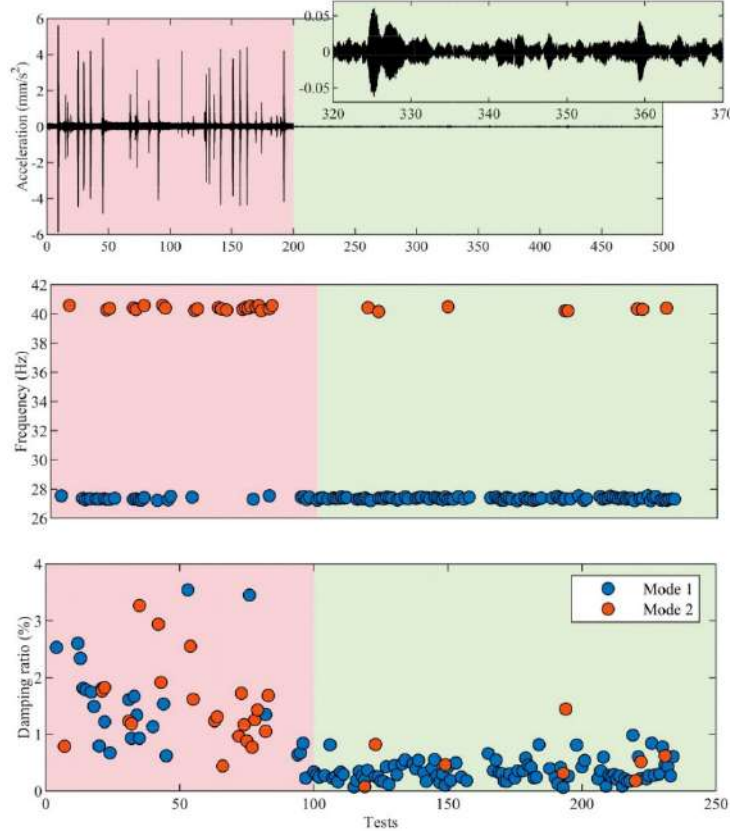


Fig. 21 Frequency and damping ratio estimation for impulsive (first 100 tests) and ambient part (second 150 tests)

used for estimating the modal parameters of the system for the ambient vibration and non-measured impulse tests. The novelty of this step-by-step methodology is the use of short OMA to determine the presence/permanence of the vibration modes throughout the entire measurement as well as study the variability of the estimates, especially in the case of the damping ratio. After several tests (i.e., trial and error method), the minimum time for OMAs has been specified in 12 seconds, with a total of 1500 samples for each part analyzed.

With this minimum time, short OMA tests have been made, applying an overlap of 50% for both the impulsive and environmental cases, obtaining a total of 234 partitions of the measure. Not all cases have presented satisfactory modal estimates. Fig. 21 shows the time history of accelerations, differentiating the impulsive part (red) and the environmental part (green), as well as the frequency and damping ratio estimates obtained in each case. It should be noted that: (i) the frequency estimate has much less variability than that of the damping ratio, (ii) there is a clear difference in the value of the estimates of the damping ratio of the impulsive case with respect to the environmental case, in the impulsive case it is they develop higher levels of damping, (iii) in the environmental case, the presence of the vertical mode is much greater than that of the radial mode, observing a greater success in their estimations in this range of the measure.

Table 1 shows a comparison between first approach and SSI-EM estimations. An excellent match is observed for the frequencies (maximum error of 1.196%). However, for the

Table 1 Modal parameters obtained

Direction	First approach		SSI-EM impulsive		SSI-EM ambiental	
	f (Hz)	ζ (%)	f (Hz)	ζ (%)	f (Hz)	ζ (%)
Vertical	27.36	1.19	27.34	1.00	27.39	0.46
Radial	40.83	0.87	40.32	1.78	40.26	0.53

Table 2 Dynamics parameters, stiffness, and damping, deduced from Table 1 and Eqs. (4) and (5)

Direction	First approach		SSI-EM impulsive		SSI-EM ambiental	
	K (N/m)	C (N/(m/s))	K (N/m)	C (N/(m/s))	K (N/m)	C (N/(m/s))
Vertical	9850.8	1.3638	9836.4	1.1452	9872.4	0.5278
Radial	21055	1.4577	21393	3.0063	21329	0.8938

damping ratio the match is not such precise. The reason lies on the logarithmic decrement method. It has been used for high amplitudes whilst OMA technique is used for the entire time record. Table 2 shows the dynamic parameters obtained from Table 1 and equations from Section 3. For the normal operation of the levitating platform, the value obtained by the SSI-EM Ambiental is more appropriate since the damping values have less variations. Thus, a vertical and radial stiffness of 9872.4 N/m and 21329 N/m, respectively, and vertical and radial damping values of

0.5278 Nm/s and 0.8938 Nm/s, respectively are measured. Resonance frequencies and damping ratios are identified at 27.39 Hz, 40.26 Hz, 0.46% and 0.53%, for vertical and radial, respectively.

7. Conclusions

The stiffness and damping of a levitating platform are revealed clearly by short Operational Modal Analysis (OMA) applications using Stochastic Subspace Identification (SSI) with Expectation Maximization (EM) technique combined with a preliminary time-frequency analysis.

Based on the results and discussions, four key conclusions can be derived. They are summarized as follows:

- (1) A passive Superconducting Magnetic Levitation (SML) system has been successfully demonstrated showing a load capacity of 4.99 N, a vertical and radial stiffness of 9872.4 N/m and 21329 N/m, respectively, and vertical and radial damping values of 0.5278 Nm/s and 0.8938 Nm/s.
- (2) This SML system can be of great application in systems like satellites or high accuracy sensors where cryogenic zones must be very well thermal isolated from hotter parts and where vibrations and micro vibrations shall be isolated.
- (3) The time-frequency analysis provides a complete perspective of the frequency operating conditions.
- (4) The SSI-EM technique has proven to be an accurate and robust method of obtaining values for frequency and damping ratio parameters for levitating platforms.
- (5) The short OMAs achieve estimations for each operating range with a reduced variation and lower uncertainty in their values.
- (6) Although the first approach has proven to be able to give a precise value of natural frequency of the system, the short OMA method must be used to obtain a quasi-instant accurate value of the operational damping of the system.

Future works will consider semi-active and active vibration isolation techniques placing coils around the magnets.

Acknowledgments

The research leading to these results has received funding from the Spanish Ministerio de Economía y Competitividad under the Plan Estatal de I+D+I 2013–2016, grant agreement n° ESP2015-72458-EXP.

References

Andersen, P. (1997), Identification of civil engineering structures using vector ARMA models, Aalborg University, Denmark.
Ashkarran, A.A. and Mahmoudi, M. (2020), “Magnetic Levitation

Systems for Disease Diagnostics”, *Trends Biotechnol.*, 1-11. <https://doi.org/10.1016/j.tibtech.2020.07.010>
Bastaitis, R., Rodrigues, G., Mokrani, B. and Preumont, A. (2009), “Active optics of large segmented mirrors: dynamics and control”, *J. Guid. Control Dyn.*, **32**(6), 1795-1803. <https://doi.org/10.2514/1.44041>
Bauer, D. (2005), “Asymptotic properties of subspace estimators”, *Automatica*, **41**(3), 359-376. <https://doi.org/10.1016/j.automatica.2004.11.012>
Busch-Vishniac, I.J. (1990), “Applications of Magnetic Levitation-Based Micro-Automation in Semiconductor Manufacturing”, *IEEE Transact. Semicond. Manuf.*, **3**(3), 109-115. <https://doi.org/10.1109/66.56563>
Cansiz, A. (2009), “Vertical, radial and drag force analysis of superconducting magnetic bearings”, *Supercond. Sci. Technol.*, **22**(7), 075003. <https://doi.org/10.1088/0953-2048/22/7/075003>
Cara, F.J., Carpio, J., Juan, J. and Alarcón, E. (2012), “An approach to operational modal analysis using the expectation maximization algorithm”, *Mech. Syst. Signal Process.*, **31**, 109-129. <https://doi.org/10.1016/j.ymsp.2012.04.004>
Casciati, F. and Domaneschi, M. (2007), “Semi-active electro-inductive devices: characterization and modelling”, *J. Vib. Control*, **13**(6), 815-838. <https://doi.org/10.1177/1077546307077465>
Casciati, F. and Giuliano, F. (2009), “Performance of multi-TMD in the towers of suspension bridges”, *J. Vib. Control*, **15**(6), 821-847. <https://doi.org/10.1177/1077546308091455>
Casciati, F., Rodellar, J. and Yildirim, U. (2012), “Active and semi-active control of structures – theory and applications: A review of recent advances”, *J. Intell. Mater. Syst. Struct.*, **23**(11), 1181-1195. <https://doi.org/10.1177/1045389X12445029>
Chang, C.M. and Chou, J.Y. (2020), “Modal tracking of seismically-excited buildings using stochastic system identification”, *Smart Struct. Syst., Int. J.*, **26**(4), 419-433. <https://doi.org/10.12989/sss.2020.26.4.419>
Chiuso, A. and Picci, G. (2004), “The asymptotic variance of subspace estimates”, *J. Econometrics*, **118**(1), 257-291. [https://doi.org/10.1016/S0304-4076\(03\)00143-X](https://doi.org/10.1016/S0304-4076(03)00143-X)
Choi, Y.M. and Gweon, D.G. (2011), “A high-precision dual-servo stage using halbach linear active magnetic bearings”, *IEEE/ASME Transact. Mechatron.*, **16**(5), 925-931. <https://doi.org/10.1109/TMECH.2010.2056694>
Díez-Jiménez, E. and Pérez-Díaz, J.L. (2011), “Flip effect in the orientation of a magnet levitating over a superconducting torus in the Meissner state”, *Physica C: Superconduct.*, **471**(1-2), 8-11. <https://doi.org/10.1016/j.physc.2010.10.008>
Díez-Jiménez, E., Sánchez-Montero, R. and Martínez-Muñoz, M. (2017), “Towards miniaturization of magnetic gears: Torque performance assessment”, *Micromachines*, **9**(1). <https://doi.org/10.3390/mi9010016>
Díez-Jiménez, E., Pérez-Díaz, J.L., Ferdeghini, C., Canepa, F., Bernini, C., Cristache, C., Sánchez-García-Casarrubios, J., Valiente-Blanco, I., Ruiz-Navas, E.M. and Martínez-Rojas, J.A. (2018), “Magnetic and morphological characterization of Nd₂Fe₁₄B magnets with different quality grades at low temperature 5–300 K”, *J. Magnet. Magnet. Mater.*, **451**, 549-553. <https://doi.org/10.1016/j.jmmm.2017.11.109>
Díez-Jiménez, E., Alcover-Sánchez, R., Pereira, E., Gómez García, M.J. and Vián, P.M. (2019a), “Design and test of cryogenic cold plate for thermal-vacuum testing of space components”, *Energies*, **14**(15). <https://doi.org/10.3390/en1215299>
Díez-Jiménez, E., Rizzo, R., Gómez-García, M.J. and Corral-Abad, E. (2019b), “Review of passive electromagnetic devices for vibration damping and isolation”, *Shock Vib.*, **2019**. <https://doi.org/10.1155/2019/1250707>
Díez-Jiménez, E., Alén-Cordero, C., Alcover-Sánchez, R. and

- Corral-Abad, E. (2021), "Modelling and test of an integrated magnetic spring-eddy current damper for space applications", *Actuators*, **10**(1), 1-18. <https://doi.org/10.3390/act10010008>
- Gauss, S., Albering, J.H., Bock, J., Kesten, M., Fieseler, H., Canders, W.R., May, H., Freyhardt, H.C. and Ullrich, M. (1999), "Cryotank with superconducting, magnetic suspension of the interior tank", *IEEE Transact. Appl. Supercond.*, **9**(2 PART 1), 1004-1007. <https://doi.org/10.1109/77.783468>
- Ghods, M., Ziaiefar, H., Mohammadzakeri, M., Omar, F.K. and Bahadur, I. (2019), "Dynamic analysis and performance optimization of permendur cantilevered energy harvester", *Smart Struct. Syst., Int. J.*, **23**(5), 421-428. <https://doi.org/10.12989/sss.2019.23.5.421>
- Hull, J.R. (2000), "Superconducting bearings", *Supercond. Sci. Technol.*, **13**, R1-R15.
- Jacobsen, N.J., Andersen, P. and Brincker, R. (2008), "Applications of frequency domain curve-fitting in the EFDD technique", *Conference Proceedings: IMAC-XXVI: A Conference & Exposition on Structural Dynamics*.
- Jamshidi, M., Chang, C.C. and Bakhshi, A. (2017), "Self-powered hybrid electromagnetic damper for cable vibration mitigation", *Smart Struct. Syst., Int. J.*, **20**(3), 285-301. <https://doi.org/10.12989/sss.2017.20.3.285>
- Jiménez-Alonso, J., Pérez-Aracil, J., Hernández Díaz, A. and Sáez, A. (2019), "Effect of Vinyl flooring on the modal properties of a steel footbridge", *Appl. Sci.*, **9**(7), 1374. <https://doi.org/10.3390/app9071374>
- Kaloo, M.R., Elsharawy, M., Abdelwahed, B., Hu, J.W. and Kim, D. (2020), "Performance assessment of bridges using short-period structural health monitoring system: Sungsu bridge case study", *Smart Struct. Syst., Int. J.*, **26**(5), 667-680. <https://doi.org/10.12989/sss.2020.26.5.667>
- Kumar, P., Huang, Y., Toyserkani, E. and Khamesee, M.B. (2020), "Development of a Magnetic Levitation System for Additive Manufacturing: Simulation Analyses", *IEEE Transact. Magn.*, **56**(8). <https://doi.org/10.1109/TMAG.2020.2997759>
- Lee, S.Y., Huynh, T.C., Dang, N.L. and Kim, J.T. (2019), "Vibration characteristics of caisson breakwater for various waves, sea levels, and foundations", *Smart Struct. Syst., Int. J.*, **24**(4), 525-539. <https://doi.org/10.12989/sss.2019.24.4.525>
- Li, J.Y., Zhu, S. and Shen, J. (2019), "Enhance the damping density of eddy current and electromagnetic dampers", *Smart Struct. Syst., Int. J.*, **24**(1), 15-26. <https://doi.org/10.12989/sss.2019.24.1.015>
- Ma, K.B., Postrekhin, Y.V. and Chu, W.K. (2003), "Superconductor and magnet levitation devices", *Rev. Sci. Instrum.*, **74**(12), 4989-5017. <https://doi.org/10.1063/1.1622973>
- MacLamore, V.R., Hart, G.C. and Stubbs, I.R. (1971), "Ambient vibration of two suspension bridges", *J. Struct. Div. (ASCE)*, **97**(ST10), 2567-2582. <https://doi.org/10.1061/JSDIAG.0003026>
- McLachlan, G. and Krishnan, T. (2007), *The EM algorithm and extensions*, Vol. 382, John Wiley & Sons.
- Niu, Y., Kraemer, P. and Fritzen, C.P. (2012), "Operational modal analysis for Canton Tower", *Smart Struct. Syst., Int. J.*, **10**(4), 393-410. <https://doi.org/10.12989/sss.2012.10.4.393>
- Ohashi, S. and Ueshima, T. (2012), "Control method of the semi-active damper coil system in the superconducting magnetically levitated bogie against vertical and pitching oscillation", *IEEE Transact. Magn.*, **48**(11), 4542-4545. <https://doi.org/10.1109/TMAG.2012.2202378>
- Olaru, R., Arcire, A., Petrescu, C., Mihai, M.M. and Gîrtan, B. (2017), "A novel vibration actuator based on active magnetic spring", *Sensors Actuators, A: Phys.*, **264**, 11-17. <https://doi.org/10.1016/j.sna.2017.07.041>
- Park, S.B. and Jang, S.J. (2020), "Design method for the 2DOF electromagnetic vibrational energy harvester", *Smart Struct. Syst., Int. J.*, **25**(4), 393-399. <https://doi.org/10.12989/sss.2020.25.4.393>
- Pérez-Díaz, J.L., García-Prada, J.C., Díez-Jiménez, E., Valiente-Blanco, I., Sander, B., Timm, L., Sánchez-García-Casarrubios, J., Serrano, J., Romera, F., Argelaguet-Vilaseca, H. and González-de-María, D. (2012), "Non-contact linear slider for cryogenic environment", *Mech. Mach. Theory*, **49**(7), 308-314. <https://doi.org/10.1016/j.mechmachtheory.2011.09.002>
- Pérez-Díaz, J., Díez-Jiménez, E., Valiente-Blanco, I., Cristache, C. and Sanchez-Garcia-Casarrubios, J. (2014a), "Contactless mechanical components: gears, torque limiters and bearings", *Machines*, **2**(3), 312-324. <https://doi.org/10.3390/machines2040312>
- Pérez-Díaz, J.L., Valiente-Blanco, I., Díez-Jiménez, E. and Sanchez-Garcia-Casarrubios, J. (2014b), "Superconducting noncontact device for precision positioning in cryogenic environments", *IEEE/ASME Transact. Mechatron.*, **19**(2), 598-605. <https://doi.org/10.1109/TMECH.2013.2250988>
- Pérez-Díaz, J.L., Díez-Jiménez, E., Valiente-Blanco, I., Cristache, C., Alvarez-Valenzuela, M.-A., Sanchez-Garcia-Casarrubios, J., Ferdeghini, C., Canepa, F., Hornig, W., Carbone, G., Plechacek, J., Amorim, A., Frederico, T., Gordo, P., Abreu, J., Sanz, V., Ruiz-Navas, E.-M. and Martínez-Rojas, J.-A. (2015), "Performance of magnetic-superconductor non-contact harmonic drive for cryogenic space applications", *Machines*, **3**(3), 138-156. <https://doi.org/10.3390/machines3030138>
- Pérez-Díaz, J.L., Valiente-Blanco, I., Cristache, C., Sanchez-García-Casarrubios, J., Rodríguez, F., Esnoz, J. and Díez-Jiménez, E. (2019), "A novel high temperature eddy current damper with enhanced performance by means of impedance matching", *Smart Mater. Struct.*, **28**(2), p. 25034. <https://doi.org/10.1088/1361-665X/aafc11>
- Preumont, A. (2018), *Vibration control of active structures: An introduction*, Springer International Publishing. <https://books.google.es/books?id=oHNLdWAAQBAJ>
- Riabzev, S., Veprik, A., Vilenchik, H. and Pundak, N. (2009), "Control of dynamic disturbances produced by a pulse tube refrigerator in a vibration-sensitive instrumentation", *Cryogenics*, **49**(1), 7-11. <https://doi.org/10.1016/j.cryogenics.2008.08.010>
- Rivin, E.I. (1995), "Vibration isolation of precision equipment", *Precision Eng.*, **17**(1), 41-56. [https://doi.org/10.1016/0141-6359\(94\)00006-L](https://doi.org/10.1016/0141-6359(94)00006-L)
- Shen, W., Zhu, S., Zhu, H. and Xu, Y.L. (2016), "Electromagnetic energy harvesting from structural vibrations during earthquakes", *Smart Struct. Syst., Int. J.*, **18**(3), 449-470. <https://doi.org/10.12989/sss.2016.18.3.449>
- Siyambalapitiya, C., De Pasquale, G. and Somà, A. (2012), "Experimental identification of rare-earth magnetic suspensions for micro and meso scale levitating systems", *Smart Struct. Syst., Int. J.*, **10**(2), 181-192. <https://doi.org/10.12989/sss.2012.10.2.181>
- Valiente-Blanco, I., Díez-Jiménez, E. and Pérez-Díaz, J.L. (2013), "Engineering and performance of a contactless linear slider based on superconducting magnetic levitation for precision positioning", *Mechatronics*, **23**(8), 1051-1060. <https://doi.org/10.1016/J.MECHATRONICS.2013.07.011>
- Valiente-Blanco, I., Díez-Jiménez, E., Cristache, C., Alvarez-Valenzuela, M.A. and Pérez-Díaz, J.L. (2014), "Characterization and improvement of axial and radial stiffness of contactless thrust superconducting magnetic bearings", *Tribology Lett.*, **54**(3), 213-220. <https://doi.org/10.1007/s11249-013-0204-0>
- Valiente-Blanco, I., Díez-Jiménez, E., Sanchez-Garcia-Casarrubios, J. and Pérez-Díaz, J.L. (2015), "Improving Resolution and Run Outs of a Superconducting Noncontact Device for Precision Positioning", *IEEE/ASME Transact.*

- Mechatron.*, **20**(4), 1992-1996.
<https://doi.org/10.1109/TMECH.2014.2351493>
- Van Overschee, P. and De Moor, B.L. (1996), *Subspace Identification for Linear Systems*, Kluwer Academic, Boston, MA, USA.
- Yu, J.H., Postrekhin, E., Ma, K.B., Chu, W.K. and Wilson, T. (1999), “Vibration isolation for space structures using HTS-magnet interaction”, *IEEE Transact. Appl. Supercond.*, **9**(2 PART 1), 908-910. <https://doi.org/10.1109/77.783444>
- Zeynalian, M., Ronagh, H.R. and Dux, P. (2012), “Analytical Description of Pinching, Degrading, and Sliding in a Bilinear Hysteretic System”, *J. Eng. Mech.*, **138**(11), 1381-1387.
[https://doi.org/10.1061/\(ASCE\)EM.1943-7889.0000442](https://doi.org/10.1061/(ASCE)EM.1943-7889.0000442)
- Zhang, T., Wang, Y. and Tamura, A. (2009), “A frequency-spatial domain decomposition (FSDD) method for operational modal analysis”, *Mech. Syst. Signal Process.*, **24**(5), 1227-1239.
<https://doi.org/10.1016/j.ymssp.2009.10.024>